Inorg. Chem. **2003**, *42*, 6194–6203

Inorganic Chemistry
Article

Synthesis and EPR Characterization of New Models for the One-Electron Reduced Molybdenum Site of Sulfite Oxidase

Katrina Peariso,[†] Balwant S. Chohan,[‡] Carl J. Carrano,*[,‡] and Martin L. Kirk*[,†]

Department of Chemistry, The University of New Mexico, MSC03 2060, 1 University of Mexico, Albuquerque, New Mexico 87131-0001, and Department of Chemistry and Biochemistry, Southwest Texas State University, San Marcos, Texas 78666

Received May 7, 2003

Deconvoluting the different contributions of thiolate and ene-1,2-dithiolate donors to the underlying electronic structure of the Mo site in sulfite oxidase (SO) has proven to be a difficult task. One way in which these differences might be illuminated is by selectively substituting Se for S in model complexes which possess multiple sulfur donor ligand environments. Here we report the synthesis and structures of new oxo–Mo(V) complexes as effective models for the one-electron reduced active site of SO. We have used the tridentate heteroscorpionate ligand (2-dimethylethanethiol)bis(3,5-dimethylpyrazolyl)methane (L3SH) in order to model the constrained cysteinyl sulfur (S_{Cys}) ligand environment observed in the crystal structure of the enzyme, and benzene-1,2-dithiol (bdt) as a mimic of the ene-1,2-dithiolate chelate. [(L3S)MoO(bdt)] and [(L3S)MoO($(SPh)_2$)] have been structurally characterized by X-ray crystallography, and as such, [(L3S)MoO(bdt)] is only the second known model compound that closely approximates the active site structure of reduced forms of SO. Additionally, benzenethiol (SPh) and benzeneselenol (SePh) have been used to perturb the equatorial ligand environment of [(L3S)MoO(bdt)].) This has provided much needed insight into the electronic structure of the one-electron reduced SO site and has allowed for increased understanding of the individual roles played by these different thiolate donors in the oxidative half-reaction of the enzyme. Interestingly, the EPR spectra of [(L3S)MoO(bdt)], [(L3S)MoO$(SPh)_2$], and [(L3S)MoO$(SePh)_2$] closely resemble that of both high pH (hpH) and low pH (lpH) SO, except for the fact that the magnitude of g_1 is found to be consistently higher in the model spectra compared to that of the enzyme. It is suggested that this derives from an increase in Mo–S covalency in the models relative to hpH and lpH SO.

Introduction

The pyranopterin molybdenum enzymes are ubiquitous in biology, performing such essential functions as the degradation of amino acids, nucleobases, and various drugs in addition to their involvement in pro-drug activation.[1] These enzymes have previously been categorized into three families, two of which are represented in mammalian systems: the xanthine oxidase (XO) and sulfite oxidase (SO) families.[1] Members of the XO family are involved in the oxidation of simple aldehydes and the hydroxylation of purines while mammalian SO converts sulfite to sulfate, presumably via an inner sphere oxygen atom transfer process. The consensus active site structures for oxidized (SO_{ox}) and reduced (SO_{red}) SO are given in Scheme 1. Both sites are pentacoordinate, possessing an apical oxo donor and equatorial ene-1,2-dithiolate and cysteine sulfur (S_{Cys}) coordination.[2−6] The five-coordinate site in SO_{ox} is completed by a second terminal oxo donor, which is replaced by water or hydroxide in reduced forms of the enzyme.[2,3,5] Catalysis is initiated in the reductive half-reaction, where the sulfite lone pair is proposed to attack the equatorial oxo donor (O_{eq}) resulting in a $2e^-$

---

* To whom correspondence should be addressed. E-mail: mkirk@unm.edu (M.L.K.).

[†] The University of New Mexico.

[‡] Southwest Texas State University.

(1) Hille, R. *Chem. Rev.* **1996**, *96*, 2757−2816.

(2) George, G. N.; Garrett, R. M.; Prince, R. C.; Rajagopalan, K. V. *J. Am. Chem. Soc.* **1996**, *118*, 8588−8592.

(3) Cramer, S. P.; Wahl, R.; Rajagopalan, K. V. *J. Am. Chem. Soc.* **1981**, *103*, 7721−7727.

(4) Huber, R.; Hof, P.; Duarte, R. O.; Moura, J. J. G.; Moura, I.; Liu, M.-Y.; LeGall, J.; Hille, R.; Archer, M.; Romao, M. J. *Proc. Natl. Acad. Sci., U.S.A.* **1996**, *93*, 8846−8851.

(5) Kisker, C.; Schindelin, H.; Pacheco, A.; Wehbi, W. A.; Garrett, R. M.; Rajagopalan, K. V.; Enemark, J. H.; Rees, D. C. *Cell* **1997**, *91*, 973−983.

(6) Enroth, C.; Eger, B. T.; Okamoto, K.; Nishino, T.; Nishino, T.; Pai, E. F. *Proc. Natl. Acad. Sci., U.S.A.* **2000**, *97*, 10723−10728.

10.1021/ic034478q CCC: $25.00

Scheme 1

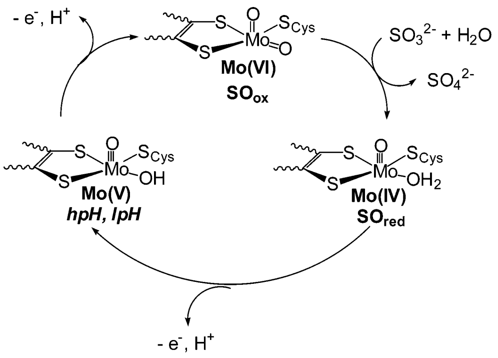

reduction of the Mo center and a subsequent transfer of O_{eq} to the substrate to form sulfate.[1,7] The oxidative half-reaction formally consists of sequential coupled electron−proton transfer steps which regenerate the oxidized active site, and the ene-1,2-dithiolate chelate has been hypothesized to a play a key role in this process by modulating the reduction potential of the Mo and/or coupling the active site into hole superexchange pathways for electron transfer regeneration of SO_{ox}.[8,9] As the coordinated cysteine is essential for catalytic activity, these same roles may also be ascribed to the S_{Cys} donor. Charge density maps of the chicken liver enzyme indicate that electrons may be sequentially transferred out of the Mo active site following docking of the b-heme domain[10] at the surface of the substrate access channel.[11,12] It has therefore been suggested that the S_{Cys}, which is directed toward this substrate access channel, could act as an electron transfer conduit between Mo and the b-type heme and facilitate the electron transfer regeneration process. As such, understanding the roles of the S_{Cys} and ene-1,2-dithiolate donors in reduced forms of SO has been a fundamental goal of researchers in this field.

Deconvoluting the different contributions of thiolate and ene-1,2-dithiolate donors to the underlying electronic structure of the Mo site in SO has proven to be a difficult task. Although Holm and co-workers[13] have recently reported the synthesis and structural characterization of $(Et_4N)[MoOCl(bdt)(2,4,6\text{-}Pr^i{}_3SC_6H_2)]$, the use of synthetic models to probe structure−property relationships that directly relate to the reduced SO active site has been hampered by the dearth of structural models that possess both ene-1,2-dithiolate and thiolate donors to molybdenum. Here we report the synthesis and structures of new oxo−Mo(V) complexes as effective models for the one-electron reduced active site of SO. We have used the tridentate heteroscorpionate ligand (2-dimethylethanethiol)bis(3,5-dimethylpyrazolyl)methane (L3SH) in order to model the constrained cysteinyl sulfur (S_{Cys}) ligand environment observed in the crystal structure of the enzyme, and benzene-1,2-dithiol (bdt) as a mimic of the ene-1,2-dithiolate chelate. As such, [(L3S)MoO(bdt)] is only the second known model compound that closely approximates the active site structure of reduced forms of SO. The incorporation of the $L3S^-$ chelate allows the O−Mo−$S_{thiolate}$−C torsion angle to be effectively constrained in these new models. This is important, as bond torsions about this angle have been shown to be critical in modulating the degree of Mo−$S_{thiolate}$ covalency in oxomolybdenum thiolate complexes, affecting the overlap between the S^v p-orbital[14] and the Mo d_{xy} redox orbital. The crystallographically determined O−Mo−S_{Cys}−C torsion angle in SO is ∼90°,[5] which is markedly different from that found in small molecule complexes such as $[MoO(SPh)_4]^{1-}$.[15] Additionally, we have used benzenethiol (SPh) and benzeneselenol (SePh) to perturb the equatorial ligand environment found in [(L3S)MoO(bdt)]. This has provided much needed insight into the electronic structure of the reduced SO site and has allowed for increased understanding of the individual roles played by these different thiolate donors during the course of catalysis.

In this manuscript, we detail the synthesis, structure, and initial spectroscopic characterization of these new model compounds in order to probe the effect of thiolate and ene-1,2-dithiolate coordination on the electronic structure of high pH (hpH) and low pH (lpH) SO and the respective abilities of these sulfur donor ligands to facilitate catalytically crucial ET processes. Additionally, the ability to directly examine electronic structure differences between thiolate and dithiolene donors in [(L3S)MoO(bdt)] and $[(L3S)MoO(SPh)_2]$ provides key insight into why nature has selected an ene-1,2-dithiolate to coordinate to molybdenum in contrast to two additional S_{Cys} donors. Finally, the judicious substitution of benzeneselenol for benzenethiol in $[(L3S)MoO(S/SePh)_2]$ shows that there is very little difference in Mo−S and Mo−Se bond covalency in this coordination environment. This allows for Se to be effectively substituted for S in mixed thiolate/dithiolate environments and used as a convenient spectroscopic probe of electronic structure due to the 4-fold increase in spin−orbit coupling between Se and S, the nearly 2:1 mass ratio, and the relatively large natural abundance of the ^{77}Se isotope ($I = {}^1/_2$, 7.56% abundance).

Experimental Section

Preparation of Compounds. All reactions were performed under a dinitrogen or argon atmosphere using standard Schlenk or drybox techniques. All manipulations were performed using solvents dried with appropriate drying agents and distilled prior to use. $(Et_4N)[MoO(SPh)_4]$ and $(Et_4N)[MoO(SePh)_4]$ were prepared by the

---

(7) Peariso, K.; McNaughton, R. L.; Kirk, M. L. *J. Am. Chem. Soc.*, in press.

(8) Inscore, F. E.; McNaughton, R. L.; Westcott, B. L.; Helton, M. E.; Jones, R.; Dhawan, I. K.; Enemark, J. H.; Kirk, M. L. *Inorg. Chem.* **1999**, *38*, 1401−1410.

(9) Helton, M. E.; Gruhn, N. E.; McNaughton, R. L.; Kirk, M. L. *Inorg. Chem.* **2000**, *39*, 2273−2278.

(10) Vertebrate SO is a homodimer. Each half of the dimer consists of a molybdenum binding domain and a heme domain that are connected by a flexible loop region.

(11) Pacheco, A.; Hazzard, J. T.; Tollin, G.; Enemark, J. H. *JBIC, J. Biol. Inorg. Chem.* **1999**, *4*, 390−401.

(12) Elliott, S. J.; McEhaney, A. E.; Feng, C.; Enemark, J. H.; Armstrong, F. A. *J. Am. Chem. Soc.* **2002**, *124*, 11612−11613.

(13) Lim, B. S.; Willer, M. W.; Miao, M.; Holm, R. H. *J. Am. Chem. Soc.* **2001**, *123*, 8343−8349.

(14) The S^v orbital is not involved in C−S σ-bonding and is orthogonal to the Mo−$S_{thiolate}$ bond.

(15) Hanson, G. R.; Brunette, A. A.; McDonell, A. C.; Murray, K. S.; Wedd, A. G. *J. Am. Chem. Soc.* **1981**, *103*, 1953−1959.

method of Bradbury et al.[16] Silica gel 60−200 mesh used in adsorption chromatography and the filtering agent Celite were obtained from the Aldrich Chemical Co. The purity of isolated compounds, as well as the progress of the reactions, was monitored by thin-layer chromatography. The ligand (2-dimethylethanethiol)-bis(3,5-dimethylpyrazolyl)methane (L3SH) was prepared using previously reported procedures.[17−19]

[(L3S)MoO(SPh)$_2$] (1). To an acetonitrile (50 mL) solution of (Et$_4$N)[MoO(SPh)$_4$] (416.8 mg, 0.614 mmol) was added L3SH (171 mg, 0.614 mmol) in the same solvent (5 mL), followed by sodium methoxide (34 mg, 0.630 mmol). The mixture was allowed to stir at room temperature for 48 h, during which time the solution changed from a deep blue to a green color. The solution was concentrated under reduced pressure by rotary evaporation (avoiding elevated temperatures). The residue was dissolved in a minimum of dichloromethane, and the products were separated by chromatography on a silica gel column (45 cm × 4 cm of silica gel, 60−200 mesh, Aldrich grade 922) using a mixture of hexane and dichloromethane as eluant. The yields were determined by weight differences following removal of solvent in preweighed flasks.

With a 4:1 mixture of dichloromethane/hexane, a yellow material identified as phenyl disulfide (34 mg) elutes rapidly from the column. The desired green monooxo product [(L3S)MoO(SPh)$_2$] elutes next with pure dichloromethane (138 mg, 37%), followed by elution of a yellow fraction identified as [(L3S)MoO$_2$Cl], (24 mg, 7%) and then finally a yellow-orange product identified as [(L3S)MoO$_2$(SPh)] (38 mg, 12%) elutes. A further insoluble red-brown material remained at the top of the column.

Crystallization of the monooxo product, [(L3S)MoO(SPh)$_2$], was accomplished by layering, in the drybox, a dichloromethane solution of the complex with hexane. Over a period of several days, thin green needlelike crystals were deposited. Anal. Calcd (Found) for $MoC_{26}H_{31}N_4S_3O{\cdot}{}^3/_4CH_2Cl_2$: C, 47.85 (47.74); H, 4.88(4.78); N, 8.34(8.32). IR (KBr disk): ν(Mo−O) 925 cm^{-1}. The most intense features of the absorption spectrum are as follows: (ν cm^{-1} (ϵ M^{-1} cm^{-1})) 14 975 (2580); 26 892 (5372).

[(L3S)MoO(SePh)$_2$] (2). The complex was synthesized in a manner similar to that described for [(L3S)MoO(SPh)$_2$]; however, as the [(L3S)MoO(SePh)$_2$] analogue is much more sensitive to air, all manipulations need to be strictly anaerobic. Crystallization of the monooxo product, [(L3S)MoO(SePh)$_2$], was accomplished by layering a dichloromethane solution of the complex with hexane. Over a period of 2 days, very thin green needlelike crystals were deposited. Anal. Calcd (Found) for $MoC_{26}H_{31}N_4SSe_2O{\cdot}{}^1/_2MeCN{\cdot}2H_2O$: C, 42.78 (42.30); H, 4.85 (4.51); N, 7.99 (8.89). IR (KBr disk): ν(Mo−O) 925 cm^{-1}. The most intense features of the absorption spectrum are as follows: (ν cm^{-1} (ϵ M^{-1} cm^{-1})) 14 008 (3302); shoulder 20 600(2250); 26 500 (5340).

[(L3S)MoO(bdt)] (3). To an acetonitrile (80 mL) solution of [(L3S)MoO(SPh)$_2$] (290 mg, 0.477 mmol) was added benzenedithiol (68 mg, 0.478 mmol). The mixture was stirred at room temperature for 3 days and then evaporated to dryness. The residue was dissolved in a minimum quantity of dichloromethane, and the products were separated by chromatography on a silica gel column using dichloromethane as an eluant. The first bright green product was the tris(benzenedithiolato)molybdenum(V) complex (34 mg, 14%). The second green product eluted was identified as unreacted [(L3S)MoO(SPh)$_2$] (102 mg, 35%). The third component was blue-green, and the product of interest was [(L3S)MoO(bdt)] (23 mg, 10%). A fourth fraction was orange and identified as [(L3S)MoO$_2$(SPh)]. A further trailing green product was identified as the monooxobis(benzenedithiolato)molybdenum(V) complex. An insoluble red-brown material remained on top of the silica column. Crystals of [(L3S)MoO(bdt)] were grown by layering a dichloromethane solution of the complex with hexane. Over a period of 3 days, dark-green block crystals were deposited. Anal. Calcd (Found) for $MoC_{20}H_{25}N_4S_3O$: C, 45.36 (44.86); H, 4.76 (4.60); N, 10.58 (10.25). IR (KBr disk): ν(Mo−O) 939 cm^{-1}. The most intense features of the absorption spectrum are as follows: (ν cm^{-1} (ϵ M^{-1} cm^{-1})) 9750 (400), 14 792 (1020); 17 908 (630); 27 900 (4760); 30 008 (4981).

Physical Methods. Elemental analyses were performed on all compounds by Quantitative Technologies, Inc., Whitehouse, NJ. All samples were dried in vacuo prior to analysis. IR spectra were recorded from KBr disks on a Perkin-Elmer 1600 series FTIR spectrometer and are reported in wavenumbers. Solution electronic absorption spectra were collected using a Hitachi-3501 UV−vis−NIR dual-beam spectrophotometer. The electronic absorption spectra were measured in 1-cm path length, black-masked, Wilmad quartz cuvettes with a Teflon stopper to prevent the introduction of O$_2$. The spectra for each of the complexes were measured using dry, degassed dichloromethane as the solvent. The measurements were repeated at a number of time points to ensure the structural stability and integrity of the complex in solution during the measurements. Cyclic voltammetric experiments were conducted using a BAS CV 50W (Bioanalytical Systems Inc., West Lafayette, IN) voltammetric analyzer. All experiments were done under argon at ambient temperature in solutions with 0.1 M tetrabutylammonium hexafluorophosphate as the supporting electrolyte. Cyclic voltammograms (CVs) were obtained using a three-electrode system consisting of platinum working, platinum wire auxiliary, and SCE reference electrodes. Potentials are reported versus the Ag/AgCl (KCl saturated) couple (197mV vs NHE). The Fc/Fc$^+$ couple was used as an internal standard to monitor the reference electrode and was observed at 578 mV (775 mV vs NHE) with $\Delta E_p = 68$mV and $i_{pc}/i_{pa} = 0.95$ in CH$_2$Cl$_2$ under similar conditions. Osteryoung square voltammograms were obtained under similar conditions with a scan rate of 200 mV/s.

XAS Measurements and Data Analysis. Mo XAS data were collected on powdered samples of [(L3S)MoO(SPh)$_2$], [(L3S)MoO(SePh)$_2$], and [(L3S)MoO(bdt)] diluted in BN at the Stanford Synchrotron Radiation Laboratory (SSRL) on beamline 7-3 using a Si(220) double-crystal monochromator detuned to 70% of the maximum intensity for harmonic rejection. All of the spectra were measured using an Ar-filled ion chamber to measure the transmitted beam intensity through the sample with the exception of [(L3S)MoO(bdt)]. Measurements were made using 10 eV increments in the pre-edge region, 0.3 eV increments in the edge region and 0.05 Å^{-1} increments in the EXAFS region with integration times of 1 s, 1 s, and 1−16 s (k^3-weighted), for a total scan time of ∼30 min. The [(L3S)MoO(bdt)] Mo EXAFS data were measured as fluorescence excitation spectra using a 30-element Ge solid-state detector array. The windowed Mo Kα count rates were ∼19 × 10^3 with a total integrated count rate of 84 × 10^3; thus, the total useful fluorescence counts per second were 2.85 × 10^6. These data were measured using 10 eV increments in the pre-edge region, 0.3 eV increments in the edge region, and 0.05 Å^{-1} increments in the EXAFS region with integration times of 1 s, 1 s, and 1−25 s (k^3-weighted), for a total scan time of ∼40 min. The temperature was

---

(16) Bradbury, J. R.; Masters, A. F.; McDonell, A. C.; Brunette, A. A.; Bond, A. M.; Wedd, A. G. *J. Am. Chem. Soc.* **1981**, *103*, 1959−1964.

(17) Hammes, B. S.; Carrano, C. J. *Inorg. Chem.* **1999**, *38*, 4593−4600.

(18) Hammes, B. S.; Carrano, C. J. *Chem. Commun.* **2000**, 1635−1636.

(19) Hammes, B. S.; Carrano, C. J. *Inorg. Chem.* **2001**, *40*, 919−927.

held at 10 K through all of the measurements using an Oxford Instruments liquid helium flow cryostat.

The XAS data were processed and analyzed using the EXAFSPAK suite of programs.[20] The X-ray energies for each of the Mo XAS spectra were calibrated by measuring the absorption spectrum of a Mo foil reference simultaneously with the transmission or fluorescence data and assigning the first inflection point of the Mo foil spectrum to 20003.9 eV. The EXAFS background correction was performed by fitting a first-order polynomial to the pre-edge region, and a three-region cubic spline through the EXAFS region. After the background was removed, the data were converted to *k*-space using $k = [2m_e(E - E_0)/\hbar^2]^{1/2}$, where $E_0 = 20025$ eV. The unfiltered EXAFS data were fit to eq 1 via a nonlinear, least-squares algorithm using theoretical amplitude and phase functions calculated for a Mo−O interaction at 1.68 Å, Mo−N at 2.21 Å, Mo−S at 2.40 Å, and Mo−Se at 2.50 Å using Feff v. 8.10.[21]

$$\chi(k) = \sum_i \frac{N_i S_i(k) A_i(k)}{kR_i^2} \exp(-2k^2\sigma_i^2)\sin(2kR_i + \phi_i(k)) \tag{1}$$

EXAFS data are described by eq 1, where $\chi(k)$ is the fractional modulation in the absorption coefficient above the edge, N_i is the number of scatterers at a distance R_i, $A_i(k)$ is the effective backscattering amplitude, σ_i^2 is the root-mean-square deviation in R_i, $\phi_i(k)$ is the phase shift experienced by the photoelectron wave in passing through the potentials of the absorbing and backscattering atoms, $S_i(k)$ is a scale factor specific to the absorber−scatterer pair, and the sum is taken over all scattering interactions. All fits were performed allowing R and σ to vary for each shell while holding the remaining parameters fixed.

EPR Measurements and Spectral Simulations. Solution and frozen glass EPR spectra were measured at X-band (∼9.3 GHz) using a Bruker EMX spectrometer. The room-temperature solution spectra were measured in dichloromethane. For the low-temperature measurements, a 1:1 toluene−dichloromethane mixture was used as a glassing solvent, and the temperature was held at 4 K in an Oxford Instruments liquid helium flow cryostat. Simulations of the EPR spectra were performed using the program QPOW.[22−24] The enzyme spectra were simulated using previously published parameters,[25,26] while removing the proton hyperfine coupling for clarity.

X-ray Crystallography. Crystal, data collection, and refinement parameters for [(L3S)MoO(SPh)$_2$] (**1**) and [(L3S)MoO(bdt)] (**3**) are given in Table 1. Crystals were sealed in thin-walled quartz capillaries. Data collection was initiated at 293 K for **3** and at 153 K for **1**. Crystals of **1** were collected at the University of Texas at Austin on a Nonius Kappa CCD diffractometer using a graphite monochromator. These crystals were extremely small in two dimensions giving weak diffraction data requiring unusually long integration times leading directly to poorer than normal *R* factors. Nevertheless, the structure was of reasonably high quality demonstrating the superior capabilities of modern CCD-based diffractometers. Crystals of **3** were mounted on a Siemens P4 diffractometer with a sealed-tube Mo X-ray source and controlled via a PC running Siemens XSCANS 2.1. The systematic absences in the diffraction data are consistent with the space groups $P2_1/c$ for **1** and *Pbca* for **3**. The structures were solved using direct methods or via the Patterson function, completed by subsequent difference Fourier syntheses, and refined by full-matrix least-squares procedures on F^2. The asymmetric unit of [(L3S)MoO(SPh)$_2$]·$^1/_2$CH$_2$Cl$_2$ contained a half solvent molecule disordered over two sites by a crystallographic inversion center. All non-hydrogen atoms (except the carbon of the disordered solvent in **1**) were refined with anisotropic displacement coefficients, while hydrogens were treated as idealized contributions using a riding model except where noted. All software and sources of the scattering factors are contained in the SHELXTL (5.0) program library (G. Sheldrick, Siemens XRD, Madison, WI). Selected bond distances and angles for the complexes are shown in Table 1 while Figures 1 and 2 contain the thermal ellipsoid diagrams of the complexes. Complete structural parameters are provided in the Supporting Information.

Table 1. Selected Bond Distances and Dihedral Angles for [(L3S)MoO(SPh)$_2$] (**1**), [(L3S)MoO(bdt)] (**3**), [(Tp*)MoO(SPh)$_2$] (**4**),[a] and [(Tp*)MoO(bdt)] (**5**)[b,c]

	1	3	4	5
	Bond Distances (Å)			
Mo(1)−N(1)	2.223(9)	2.176(5)	2.164(5)	2.179(5)
Mo(1)−N(2)			2.207(5)	2.178(5)
Mo(1)−N(3)	2.426(9)	2.521(6)	2.357(5)	2.372(4)
Mo(1)−O(1)	1.676(7)	1.657(5)	1.676(4)	1.678(4)
Mo(1)−S(1)	2.401(3)	2.380(2)		
Mo(1)−S(2)	2.429(3)	2.370(2)	2.383(2)	2.368(2)
Mo(1)−S(3)	2.376(4)	2.400(2)	2.380(2)	2.379(2)
	Dihedral Angles (deg)			
O(1)−Mo(1)−S(3)−C	−41.49	+81.82		
O(1)−Mo(1)−S(2)−C	−65.79	−79.26		
O(1)−Mo(1)−S(1)−C	−106.51	+115.10		

[a] See ref 27. [b] See ref 28. [c] Numbers in parentheses are the estimated standard deviation.

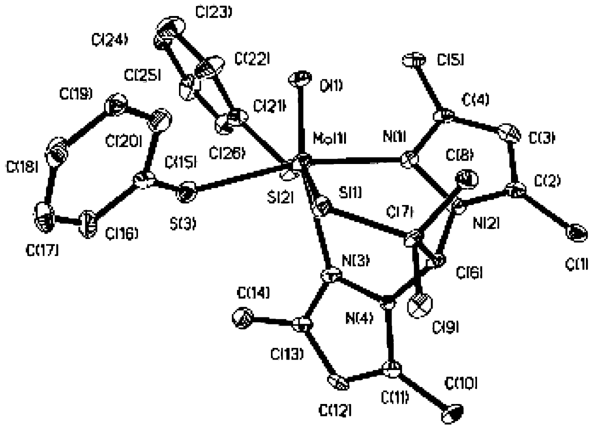

Figure 1. ORTEP diagram with 20% thermal ellipsoids for [(L3S)MoO(SPh)$_2$] (**1**) showing complete atomic labeling.

Results and Analysis

Solid-State Structures of the Complexes. As expected, the molecular structures of [(L3S)MoO(SPh)$_2$] (Figure 1) and [(L3S)MoO(bdt)] (Figure 2) clearly show that the two pyrazolyl nitrogens and one thiolate sulfur of the (L3S)$^-$ ligand are facially coordinated. Although the Mo(V) ion is ostensibly six-coordinate, the structure can perhaps be better described as a 5 + 1 square pyramid due to the extensive lengthening of the Mo−N(3) bond resulting from a strong

---

(20) George, G. N. Stanford Synchrotron Radiation Laboratory: Menlo Park, 2000.
(21) Rehr, J. J.; Albers, R. C. *Rev. Mod. Phys.* **2000**, *72*, 621−654.
(22) Nilges, M. J. In *Chemistry*; University of Illinois: Urbana, Illinois, 1979.
(23) Belford, R. L.; Nilges, M. J. In *21st Rocky Mountain Conference*; Denver, CO, 1979.
(24) Maurice, A. M. In *Chemistry*; University of Illinois: Urbana, Illinois, 1980.
(25) Dhawan, I.; Enemark, J. H. *Inorg. Chem.* **1996**, *35*, 4873−4882.
(26) George, G. N.; Bray, R. C. *Biochemistry* **1988**, *27*, 3603−3609.

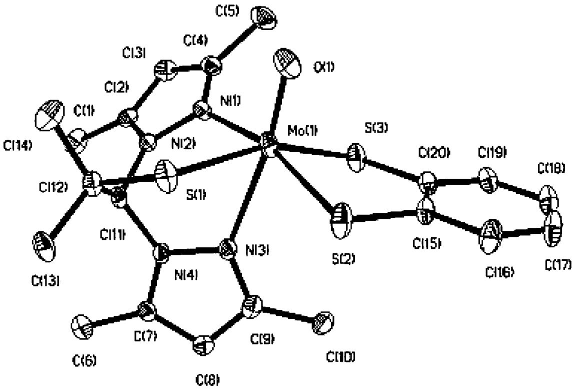

Figure 2. ORTEP diagram with 20% thermal ellipsoids for [(L3S)MoO(bdt)] (**3**) showing complete atomic labeling.

Table 2. Redox Potentials of Complexes Prepared in This Study[a]

species	E_p	ΔE_p	i_{pa}/i_{pc}
[(L3S)MoO(SePh)$_2$]	−424	64	1.01
	+612	78	0.05
[(L3S)MoO(SPh)$_2$]	−424	67	0.93
	+768	62	0.78
[(L3S)MoO(bdt)]	−364	76	0.92
	+796	72	0.65

[a] For conditions, see text.

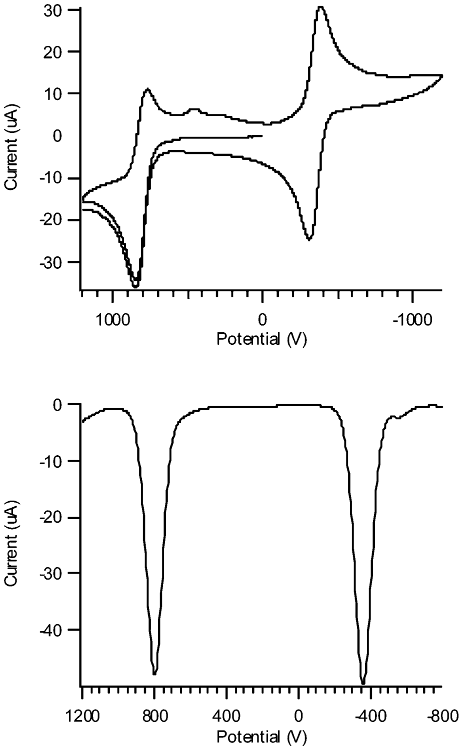

Figure 3. Cyclic voltamogram (scan rate 200 mv/s) of [(L3S)MoO(bdt)] using conditions as described in the text (upper). Osteryoung sqare wave voltammogram(lower).

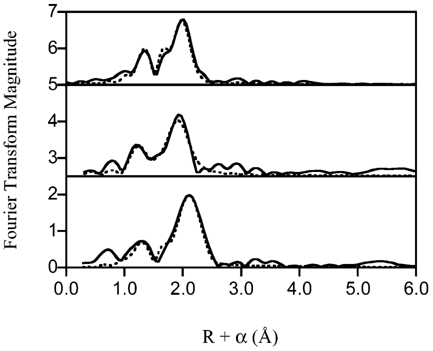

Figure 4. Fourier transformed Mo EXAFS data for [(L3S)MoO(bdt)] (top), [(L3S)MoO(SPh)$_2$] (middle), and [(L3S)MoO(SePh)$_2$] (bottom).

structural trans effect due to the oxo ligand. Thus, while the Mo−N(1) bonds average 2.189(9) Å in [(L3S)MoO(bdt)], [(L3S)MoO(SPh)$_2$], and the Tp* analogues, [Tp*MoO(bdt)][28] and [Tp*MoO(SPh)$_2$],[27] the trans Mo(V)−N$_{pz}$ bond lengths are 2.521, 2.426, 2.372, and 2.357 Å, respectively (Table 1). Especially notable is the very long distance recorded for the Mo−N(3) bond in the [(L3S)MoO(bdt)] derivative which is over 0.3 Å longer than the cis Mo−N bond. In each case, the Mo atom lies above the center of a square plane consisting of N(1), S(1), S(2), and S(3). The oxo oxygen O(1) is orthogonal to this plane, and the Mo lies approximately 0.3−0.4 Å out of plane toward the apical oxo. The important O−Mo−S−C dihedral angles are summarized in Table 1. The O−Mo−S(1)−C dihedral angle involving the thiolate from the L3S ligand possesses an average value of 111°. It should be noted that the structure of the L3S ligand effectively constrains this angle in [(L3S)MoO(SPh)$_2$] and [(L3S)MoO(bdt)] to within 4° of the average. The other dihedral angles involving the thiophenol and bdt sulfurs are substantially different.

Electrochemistry. The electrochemical behavior of [(L3S)MoO(SePh)$_2$], [(L3S)MoO(SPh)$_2$], and [(L3S)MoO(bdt)] were examined by cyclic voltammetry (CV) and Osteryoung square wave voltammetry. The results for the cyclic voltammetric experiments are presented in Table 2, and the cyclic voltammogram of [(L3S)MoO(bdt)] is shown in Figure 3. All three complexes show a quasireversible wave between −350 and −450 mV versus SCE in CH_2Cl_2, corresponding to the one-electron reduction of Mo(V) to Mo(IV). Also observed are oxidation waves in the +600 to +800 mV range resulting from the oxidation of Mo(V) to Mo(VI). These oxidations range from quasireversible in the case of the thiophenol and bdt derivatives to nearly irreversible for [(L3S)MoO(SePh)$_2$]. One-electron oxidations of Mo(V) complexes are often irreversible due to the inherent instability of mono-oxo Mo(VI) to the addition of a second oxo group from traces of water in the solvent, resulting in a considerably more stable dioxo $[MoO_2]^{2+}$ moiety.

EXAFS. [(L3S)MoO(SePh)$_2$] did not produce crystals of sufficient quality for X-ray crystallography. Thus, in lieu of crystallographic characterization, EXAFS spectra were measured in the solid state for all three complexes to characterize the structure of [(L3S)MoO(SePh)$_2$] and compare the EXAFS determined bond distances with that of [(L3S)MoO(SPh)$_2$] and [(L3S)MoO(bdt)]. The Fourier transformed EXAFS data (Figure 4) for all three complexes show two distinct peaks; however, the main peak in the [(L3S)MoO(SePh)$_2$] spectrum

---

(27) Cleland, W. E., Jr.; Barnhart, K. M.; Yamanouchi, K.; Collison, D.; Mabbs, F. E.; Ortega, R. B.; Enemark, J. H. *Inorg. Chem.* **1987**, *26*, 1017−1025.

(28) Dhawan, I. K.; Pacheco, A.; Enemark, J. H. *J. Am. Chem. Soc.* **1994**, *116*, 7911−7912.

Table 3. EXAFS Fitting Results for (L3S)MoO(bdt), (L3S)MoO(SPh)$_2$, and (L3S)MoO(SePh)$_2$ Models[a−c]

	shell 1			shell 2			shell 3/4		
	N	R_{ab} (Å)	$\sigma^2 \times 10^3$ (Å^2)	N	R_{ab} (Å)	$\sigma^2 \times 10^3$ (Å^2)	N	R_{ab} (Å)	$\sigma^2 \times 10^3$ (Å^2)
[(L3S)MoO(bdt)]	1O	1.69	1.0	1N	2.19	1.3	3S	2.40	1.9
[(L3S)MoO(SPh)$_2$]	1O	1.65	1.5	1N	2.17	11.5	3S	2.40	2.8
[(L3S)MoO(SePh)$_2$]	1O	1.67	2.3	1N	2.18	5.4	1S	2.39	1.5
							2Se	2.53	3.3

[a] Parameters given are from fits to unfiltered data. [b] The axial N ligand was not included in the fits because it is a significantly weaker scatterer than the thiolates, and it occurs at an unresolvable distance from that of the thiolate shell in [(L3S)MoO(SPh)$_2$]. [c] $S_i(k) = 0.9$ and $\Delta E_0 = -8$ for all of the fits.

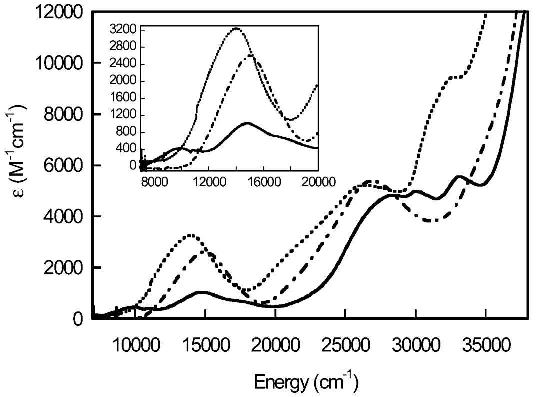

Figure 5. Solution electronic absorption spectra of [(L3S)MoO(bdt)] (—), [(L3S)MoO(SPh)$_2$] (− • −), and [(L3S)MoO(SePh)$_2$] (···). The spectra were measured at room temperature in CH$_2$Cl$_2$. The inset more clearly displays the region between 7000 cm^{-1} and 20 000 cm^{-1}.

has a significantly higher amplitude and is shifted to a longer distance (ΔR = 0.1 Å) than those observed for [(L3S)MoO(bdt)] and [(L3S)MoO(SPh)$_2$]. This higher amplitude and longer distance are indicative of the differences that are expected upon exchanging a thiolate for a selenolate donor. These differences are also evident in the fits to the data (Table 3). All three complexes are well modeled with the first 2 shells containing 1O at 1.67 Å and 1N at ∼2.18 Å, respectively (the expected contribution from the pyrazole nitrogen trans to the oxo is not observed since it is at a sufficiently long distance that it does not materially affect the EXAFS). The third shells for both the [(L3S)MoO(bdt)] and [(L3S)MoO(SPh)$_2$] complexes are best modeled with a single shell of 3S at ∼2.4 Å, consistent with the crystallographic data. In contrast, [(L3S)MoO(SePh)$_2$] requires a shell of 1S at ∼2.4 Å and a shell of 2Se scatterers at 2.52 Å to adequately model the data. The minimal differences observed in the EXAFS data for [(L3S)MoO(bdt)], [(L3S)MoO(SPh)$_2$], and mixed molybdenum thiolate/selenolate, [(L3S)MoO(SePh)$_2$], offer compelling evidence to suggest that the structures of all three complexes are very similar with the only differences originating from the expected changes accompanying a thiolate to selenolate substitution.

Electronic Absorption Spectra. The electronic absorption spectra of [(L3S)MoO(bdt)], [(L3S)MoO(SPh)$_2$], and [(L3S)MoO(SePh)$_2$] demonstrate how differences in the nature of the equatorial donor ligands affect significant changes in the electronic structure of these complexes (Figure 5). The absorption spectra of [(L3S)MoO(SPh)$_2$] and [(L3S)MoO(SePh)$_2$] are relatively similar to one another below ∼30 000 cm^{-1}. Both spectra have two strong absorption bands with maxima at 14 975 and 26 890 cm^{-1} for [(L3S)MoO(SPh)$_2$] and similar, slightly red-shifted bands at 14 008 and 26 500 cm^{-1} for [(L3S)MoO(SePh)$_2$]. The shoulder observed at ∼20 600 cm^{-1} (ϵ = 2250 M^{-1} cm^{-1}) in the [(L3S)MoO(SePh)$_2$] spectrum is tentatively assigned as a Se → Mo $d_{xz,yz}$ LMCT transition that is red-shifted from that of [(L3S)MoO(SPh)$_2$]. A similar transition is most likely present at higher energy in the [(L3S)MoO(SPh)$_2$] spectrum but is obscured under the 26 890 cm^{-1} band. The lower energy bands at 14 008 and 14 975 cm^{-1} are similar to those observed in (Et$_4$N)[MoO(SePh)$_4$] and (Et$_4$N)[MoO(SPh)$_4$][16,29] which have been previously assigned as S^v/Se^v → Mo d_{xy} LMCT transitions.[14] The ∼3000 M^{-1} cm^{-1} extinction coefficient observed for these S/Se^v → Mo d_{xy} LMCT bands in [(L3S)MoO(SPh)$_2$] and [(L3S)MoO(SePh)$_2$] is approximately half that observed for [MoO(SPh)$_4$]$^-$ and [MoO(SePh)$_4$]$^-$.[15] This is consistent with the presence of only two thiolate/selenolate ligands in [(L3S)MoO(SPh)$_2$] and [(L3S)MoO(SePh)$_2$] possessing O$_{ax}$−Mo−S$_{thiolate}$−C dihedral angles that are similar to those observed in [MoO(SPh)$_4$]$^-$ and [MoO(SePh)$_4$]$^-$. This suggests that the constrained dihedral angle of ∼110° in the (L3S) thiolate ligand precludes a significant overlap with the Mo d_{xy} orbital, resulting in a substantial reduction in L3S S^v → Mo d_{xy} charge transfer intensity.

While the absorption spectra of [(L3S)MoO(SPh)$_2$] and [(L3S)MoO(SePh)$_2$] are very similar, changing the equatorial ligand to benzene-1,2-dithiolate causes significant changes in the low energy region of the spectrum (Figure 5, inset). In contrast to the single, broad low energy feature found in both the dithiolate and diselenolate spectra,[30] there are three distinct, lower intensity features in the [(L3S)MoO(bdt)] spectrum at 9750 cm^{-1} (ϵ = 400 M^{-1} cm^{-1}), 14 792 cm^{-1} (ϵ = 1020 M^{-1} cm^{-1}) and 17 908 cm^{-1} (ϵ = 630 M^{-1} cm^{-1}). Three charge transfer bands have been reported in a similar energy region for [Tp*MoO(bdt)].[8] The weak $d_{xy}-d_{xz,yz}$ ligand field transition is not observed and is almost certainly obscured beneath the ∼14 800 cm^{-1} band in [(L3S)MoO(bdt)] and [Tp*MoO(bdt)] (where Tp* = hydrotris-(3,5-dimethyl-1-pyrazolyl)borate). Interestingly, the relative intensities of the transitions observed at 14 792 and 17 980 cm^{-1} in [(L3S)MoO(bdt)] are reversed from those

---

(29) McNaughton, R. L.; Tipton, A. A.; Rubie, N. D.; Conry, R. R.; Kirk, M. L. *Inorg. Chem.* **2000**, *39*, 5697−5706.

(30) It should be noted that the bandwidth of [(L3S)MoO(SPh)$_2$] and [(L3S)MoO(SePh)$_2$] are slightly broadened due to some populations of other rotamers with varying torsion angles. The reader should consult ref 29 for additional details.

Table 4. Comparison of EPR Parameters for Oxomolybdenum(V) Complexes and Pyranopterin Molybdenum Enzymes[a]

sample	g_1	g_2	g_3	$\langle g \rangle$	A_1	A_2	A_3	$\langle A \rangle$	α	β	γ	ref
[(L3S)MoO(SPh)$_2$]	2.014	1.966	1.946	1.976	55	29	27	35	8	30	0	*b*
[(L3S)MoO(SePh)$_2$]	2.084	1.977	1.943	1.979	52	28	23	37	8	30	0	*b*
[(L3S)MoO(bdt)]	2.016	1.972	1.949	1.979	52	26	24	34	8	40	0	*b*
Xanthine Oxidase												
very rapid (xanthine)	2.025	1.955	1.949	1.976	44.4	18.2	19.1	27.2	0	18	0	22
rapid type I (formamide)	1.989	1.969	1.965	1.974	61.4	24.7	25.7	37.3	0	20	0	22
Sulfite Oxidase												
high pH	1.990	1.966	1.954	1.970	54.4	21.0	11.3	28.9	0	14	22	21
low pH	2.007	1.974	1.968	1.983	56.7	25.0	16.7	32.8	0	18	0	21

[a] ^{95,97}Mo hyperfine parameters reported in units of 10^{-4} cm^{-1}. [b] Values obtained from this work.

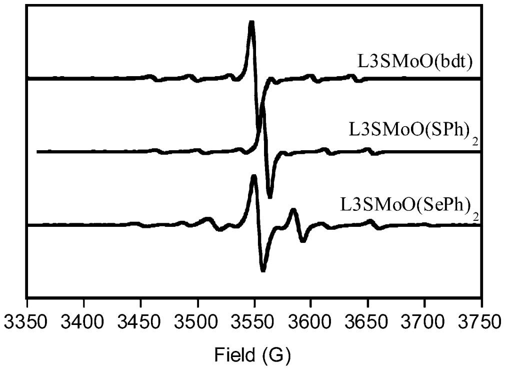

Figure 6. Isotropic X-band EPR data for [(L3S)MoO(bdt)] (top), [(L3S)MoO(SPh)$_2$] (middle), and [(L3S)MoO(SePh)$_2$] (bottom).

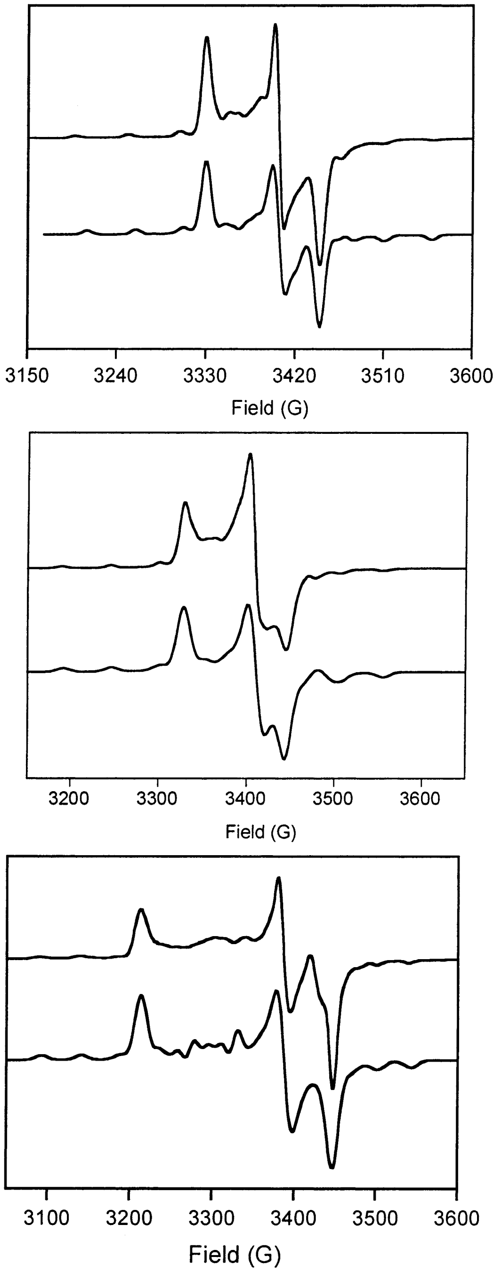

Figure 7. The 4 K EPR spectra (upper plot in each window) and simulations (lower plot in each window) for [(L3S)MoO(bdt)] (top), [(L3S)MoO(SPh)$_2$] (middle), and [(L3S)MoO(SePh)$_2$] (bottom).

observed in [Tp*MoO(bdt)]. This may be due, in part, to a small L3S $S^v \rightarrow$ Mo d_{xy} LMCT contribution to the intensity of the band at 14 792 cm^{-1} in the [(L3S)MoO(bdt)] model that is not present in the [Tp*MoO(bdt)] complex. Despite these minor differences, it is reasonable to suggest that all three of these bands arise from S → Mo LMCT transitions.[8] Thus, changing the equatorial ligation from two thiolate donors to an ene-1,2-dithiolate chelate has effectively separated and lowered the energies of the S → Mo LMCT manifold, allowing for the resolution of one broad feature in [(L3S)MoO(SPh)$_2$] into three distinct transitions for [(L3S)MoO(bdt)]. This likely reflects the different valence ionization energies of dithiolate and thiolate donors. The significant decrease in charge transfer intensity between [(L3S)MoO(SPh)$_2$] and [(L3S)MoO(bdt)] is also consistent with a decrease in Mo−S bond covalency between thiolates and dithiolate (dithiolene) donors.[29,31]

EPR Spectroscopy. The differences in electronic structure resulting from changes in the equatorial ligation are also evident in the EPR spectra. The isotropic solution EPR data (Figure 6) all show a prominent ^{98}Mo signal at $g \sim 2$ and the six ^{95,97}Mo ($I = {}^5/_2$; 25.38% abundance) hyperfine lines. There are two additional lines observed in the spectrum of [(L3S)MoO(SePh)$_2$] that are centered around the ^{98}Mo signal and split by 73.5 G. These features are most likely ligand hyperfine coupling between the ^{98}Mo and the ^{77}Se nucleus ($I = {}^1/_2$; 7.56% abundance). While slight shifts in the isotropic g-values are observed in the room-temperature spectra (Table 4), more dramatic changes reflecting differences in M−L covalency and spin−orbit coupling are observed in the low-temperature anisotropic spectra (Figure 7).

The three spectra displayed in Figure 7 all have g_1 values (Table 4) greater than the free electron value, g_e, and this is

---

(31) McNaughton, R. L.; Helton, M. E.; Rubie, N. D.; Kirk, M. L. *Inorg. Chem.* **2000**, *39*, 4386-4387.

consistent with previously reported EPR spectra of d^1 oxo−Mo thiolate complexes with multiple thiolate donors.[15,16,25,32,33] Westmoreland and co-workers[32,34,35] have shown in studies of oxo−molybdenum halide complexes that there are three fundamental contributions that can lead to g_1 values that are greater than g_e, and these are large metal−ligand covalencies, large ligand spin−orbit coupling, and the presence of low energy LMCT states. The electronic absorption spectra for the three complexes in this study clearly show the presence of low energy LMCT transitions, with the lowest energy transitions being present in [(L3S)MoO(bdt)]. While the g_1 values for [(L3S)MoO(bdt)] and [(L3S)MoO(SPh)$_2$] are nearly identical, replacing the thiolates with selenolate donors results in a dramatic increase in g_1 due to the significant increase in the ligand spin−orbit coupling constant ($\zeta_S = 374$ cm^{-1} and $\zeta_{Se} = 1650$ cm^{-1}).[36] The g_2 and g_3 values for [(L3S)MoO(bdt)] and [(L3S)MoO(SPh)$_2$] are relatively similar, while g_2 and g_3 for [(L3S)MoO(SePh)$_2$] clearly indicate that this complex is considerably more rhombic. The resolution at X-band was insufficient to directly determine the A_2 and A_3 values for [(L3S)MoO(SPh)$_2$], [(L3S)MoO(SePh)$_2$], and [(L3S)MoO(bdt)]; however, the best simulations were obtained with the values given in Table 4.

Discussion

We have presented the synthesis and initial spectroscopic characterization of novel mixed-ligand complexes as models for the one-electron reduced active site of SO. Crystallographic characterization of these complexes has shown that [(L3S)MoO(SPh)$_2$], and [(L3S)MoO(bdt)] possess three S-donors in the equatorial plane, consistent with the consensus active site structure for SO.[2,5] While the use of the tridentate L3S$^-$ ligand necessarily produces a six-coordinate complex, the orientation of the pyrazole nitrogen trans to the strong oxo donor results in a significantly longer (>0.2 Å) Mo−N$_{ax}$ bond distance than the ~2.18 Å distance observed for Mo−N$_{eq}$. This suggests that the Mo−N$_{ax}$ bonding interaction does not contribute significantly to the overall electronic structure of the complexes. The L3S$^-$ ligand also effectively constrains the O−Mo−S$_{thiolate}$−C dihedral angle in [(L3S)MoO(bdt)] and [(L3S)MoO(SPh)$_2$] to ~111°, which is closer to the ~90° angle determined for chicken SO[5] than one might be expected to obtain using unconstrained thiolate donors.

The similarity of the electronic absorption spectra for [(L3S)MoO(SPh)$_2$] and [(L3S)MoO(SePh)$_2$] demonstrates that there is very little difference in the underlying electronic structure of these complexes, despite changing two of the equatorial ligands from thiolate to selenolate donors. Additionally, the ability to directly examine electronic structure differences between thiolate and dithiolene donors in [(L3S)MoO(bdt)] and [(L3S)MoO(SPh)$_2$] has allowed for insight into why nature has selected an ene-1,2-dithiolate to coordinate to molybdenum in contrast to two additional S$_{Cys}$ donors. A comparison of the electronic absorption spectra for [(L3S)MoO(SPh)$_2$] and [(L3S)MoO(bdt)] clearly shows that significant differences exist between thiolate and dithiolene donors, and this undoubtedly has a profound effect on properly tuning the electronic structure of the Mo center in SO. The electronic structure differences between [(L3S)MoO(SPh)$_2$] and [(L3S)MoO(bdt)] are also reflected in the electrochemical data, which show that [(L3S)MoO(bdt)] ($E_{1/2}$red = −364 mV) is ~60 mV easier to reduce than [(L3S)MoO(SPh)$_2$] ($E_{1/2}$red = −424 mV). This is an interesting result, as it would imply that the coordination of three S$_{cys}$ donors to Mo in SO$_{ox}$ (as opposed to one S$_{Cys}$ and an ene-1,2-diothiolate) may thermodynamically destabilize SO$_{red}$ and inhibit the atom transfer step of the reductive half-reaction.[37] There are also implications regarding the electron transfer half-reaction as well. Our results indicate that one-electron oxidation of SO$_{red}$ to the Mo(V) level may be more thermodynamically uphill than if three S$_{Cys}$ donors were bound to the Mo site. However, the potential differences between the [Mo^{IV}O(ene-1,2-dithiolate)(S$_{Cys}$)(OH$_2$)]$^-$ SO$_{red}$ site and a hypothetical [Mo^{IV}O(S$_{Cys}$)$_3$(OH$_2$)]$^-$ site with respect to the thermodynamics of electron transfer could be overshadowed by the proposed coupled electron−proton transfer event associated with the Mo^{IV} → Mo^V conversion of Scheme 1.

The inherent electronic structure differences between [(L3S)MoO(SPh)$_2$], [(L3S)MoO(SePh)$_2$], and [(L3S)MoO(bdt)] are also apparent in the EPR spectra of these complexes. Appreciable differences in **g**-tensor anisotropy are observed in the low-temperature EPR spectra of [(L3S)MoO(SePh)$_2$] and [(L3S)MoO(SPh)$_2$]. This is interesting, since these complexes possess nearly identical electronic absorption spectra, which indicate that the charge transfer manifolds of these two complexes are virtually the same. Since **g**-tensor anisotropy is a function of both the energy of these LMCT states and their ability to spin−orbit couple with the ground state,[38] to first order the EPR spectral differences are simply a function of the ligand spin−orbit coupling constant. In addition, it is worth noting that $g_{iso} \neq g_{ave}$ in the EPR spectra of [(L3S)MoO(SePh)$_2$]. This may be due, in part, to the variability of the O−Mo−Se−C torsion angles in the isotropic EPR spectrum, while the frozen solution would have predominantly one, minimum-energy conformation, such as that found in the solid-state crystal structure of [(L3S)MoO(SPh)$_2$]. A conformation that possessed O−Mo−Se−C torsion angles that deviate significantly from 270° (90°) would provide better Se-p Mo d_{xy}[29] orbital overlap, increasing $\mathbf{g}_1$ and producing $g_{ave} > g_{iso}$. Variable temperature-variable frequency EPR studies are

---

(32) Balagopalakrishna, C.; Kimbrough, J. T.; Westmoreland, T. D. *Inorg. Chem.* **1996**, *35*, 7758−7768.

(33) Mader, M. L.; Carducci, M. D.; Enemark, J. H. *Inorg. Chem.* **2000**, *39*, 525−531.

(34) Swann, J.; Westmoreland, T. D. *Inorg. Chem.* **1997**, *36*, 5348−5357.

(35) Niaples, N. S.; Westmoreland, T. D. *Inorg. Chem.* **1997**, *36*, 756−757.

(36) Mabbs, F. E.; Collison, D. *Electron Paramagnetic Resonance of d Transition Metal Compounds*; Elsevier: Amsterdam, 1992; Vol. 16.

(37) Tucci, G. C.; Donahue, J. P.; Holm, R. H. *Inorg. Chem.* **1998**, *37*, 1602−1608.

(38) The LF energies are assumed, and anticipated, to be virtually identical for [(L3S)MoO(SePh)$_2$] and [(L3S)MoO(SPh)$_2$].

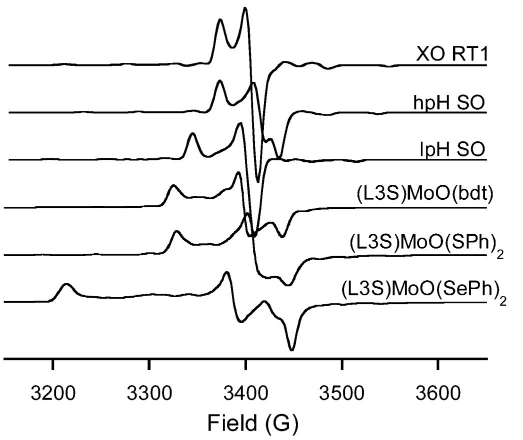

Figure 8. The 4 K X-band EPR spectra of [(L3S)MoO(bdt)], [(L3S)MoO$(SPh)_2$], and [(L3S)MoO$(SePh)_2$] and simulations of the XO rapid type 1, hpH SO, and lpH SO. Enzyme simulations were performed using previously reported Mo parameters.[21,26] The proton hyperfine coupling reported for the rapid type 1 was not included in the simulations so that the Mo contributions to the spectra could be easily compared with those of the models.

currently underway to examine the structural differences that could give rise to $g_{ave} > g_{iso}$.

In contrast to the [(L3S)MoO$(SPh)_2$] and [(L3S)MoO$(SePh)_2$] spectra, the EPR spectra of [(L3S)MoO(bdt)] and [L3S)MoO$(SPh)_2$] are relatively similar, despite the obvious differences in sulfur donor ligands and electronic absorption spectra. The nearly identical g_1 values observed for [(L3S)MoO(bdt)] and [(L3S)MoO$(SPh)_2$] suggest that the lower energy charge transfer state observed at 9750 cm^{-1} in [(L3S)MoO(bdt)] compensates for the decreased Mo−S bond covalency in this complex. This result demonstrates the importance of d^1 oxo−molybdenum thiolate electronic structure to the analysis of magnetic resonance data, since both metal−ligand covalency and the energy of low-lying LMCT states contribute significantly to the observed **g**-tensor anisotropy.[32,34]

Although [(L3S)MoO(bdt)] and [(L3S)MoO$(SPh)_2$] display similar g_1 values, the increased rhombicity observed in the [(L3S)MoO(bdt)] EPR spectrum may offer insight into the geometric structures of hpH and lpH SO as well as reduced forms of XO.[3,6] Anisotropic EPR data for [(L3S)MoO(bdt)], [(L3S)MoO$(SPh)_2$], and [(L3S)MoO$(SePh)_2$] together with simulations of previously reported spectra for hpH SO, lpH SO, and XO rapid type 1 are presented in Figure 8.[25,26] Here it is readily noticed that g_1 for lpH SO is greater than g_e, similar to that of [(L3S)MoO(bdt)] and [(L3S)MoO$(SPh)_2$], while g_1 values for hpH SO and the XO_{RT1} signal are significantly lowered, yielding $g_1 < g_e$. These data address two important points regarding SO and XO. Despite the apparent similarity between the coordination environment of [(L3S)MoO(bdt)] and hpH and lpH SO, the metal−ligand interactions that define the ground state electronic structure of hpH SO are more similar to those of XO_{RT1} than that of either the lpH SO or [(L3S)MoO(bdt)]. Second, the similar EPR spectra observed for XO_{RT1} and hpH SO support a proposal that, during enzymatic turnover, it is the terminal oxo ligand in XO that occupies the apical position.[39] This is an important point, as considerable controversy exists regarding the orientation of the terminal oxo and catalytically essential sulfido ligands in XO (Scheme 2).[6] From a stereochemical point of view, it is difficult to imagine how the equatorial oxo ligand proposed for XO_{ox} could rearrange to occupy an apical position in XO_{RT1}.

Scheme 2

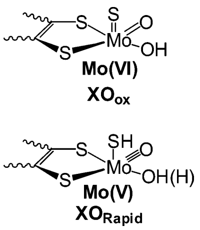

With the oxo in the apical position, the similarity in g_1 between hpH SO and XO_{RT1} could then be accounted for by similar Mo-equatorial thiolate donor covalency in the Mo^V state of the enzymes. George et al.[26] have shown that the XO_{RT1} EPR signal has an unusually large proton hyperfine coupling. This is the anticipated result provided the sulfhydryl proton is oriented in the equatorial plane, resulting in an O_{ax}−Mo−S−H dihedral angle of ~90°. Therefore, the strong hyperfine coupling originating from the equatorial sulfhydryl proton in XO_{RT1} may hold the key to understanding the strong similarity in g_1 between this XO enzyme form and hpH SO. Any significant deviation of the sulfhydryl proton out of the equatorial plane in XO_{RT1} would result in a concomitant decrease in the ^1H hyperfine interaction and a corresponding increase in the covalency of the Mo d_{xy}−S p interaction. As was mentioned earlier, the O_{ax}−Mo−S_{Cys}−C dihedral angle in chicken SO[5] is ~90°, which implies very weak overlap between the Mo d_{xy} and S^{v}_{Cys} p orbitals.[29] These arguments are in complete agreement with the work of Westmoreland and co-workers, who have quantitated the effect of covalency on the magnitude of g_1 and shown that removing the covalency contribution to **g**-tensor anisotropy will consistently give $g_1 \leq g_e$.[32,34]

While the magnitude of g_1 in XO_{RT1} and hpH SO can be accounted for with experimental evidence, the origin of why $g_1 > g_e$ for lpH SO_{red} is not so readily evident. On the basis of the arguments presented, an observed increase in g_1 is most likely a manifestation of a change in the O_{ax}−Mo−S_{Cys}−C dihedral angle brought about by the change in pH. Astashkin et al.[40] have suggested that the equatorial oxygen donor is protonated in lpH SO, and that this proton forms a hydrogen bond to the S_{Cys} atom. This hydrogen bonding interaction could distort the O_{ax}−Mo−S_{Cys}−C dihedral angle away from the crystallographically observed value of ~90°, resulting in increased Mo d_{xy}−S_{Cys} p orbital overlap. In summary, the magnitude of g_1 provides insight into the electronic structure of EPR active forms of mammalian XO and SO that cannot be directly obtained from electronic absorption spectroscopy due to complications arising from other endogenous chromophores, which preclude the ability to collect clean and interpretable charge transfer spectra.

---

(39) Jones, R. M.; Inscore, F. E.; Hille, R.; Kirk, M. L. *Inorg. Chem.* **1999**, *38*, 4963−4970.

(40) Astashkin, A. V.; Mader, M. L.; Pacheco, A.; Enemark, J. H.; Raitsimring, A. M. *J. Am. Chem. Soc.* **2000**, *122*, 5294−5302.

The spectroscopic data presented for [(L3S)MoO(bdt)], [(L3S)MoO(SPh)$_2$], and [(L3S)MoO(SePh)$_2$] provide an initial basis for the interpretation of enzyme EPR spectra. However, specific spectral differences are observed between the models and the enzymes. Of particular importance is the fact that $g_1 > g_e$ for all of the model systems. This may be due to the fact that the O−Mo−S$_{\text{thiolate}}$−C dihedral angle in the models is more obtuse than that observed in the structure of SO, where this angle was found to be ∼90°. Bond torsions about this angle have been shown to be critical in modulating the degree of Mo−S$_{\text{thiolate}}$ covalency in oxomolybdenum thiolate complexes, affecting the overlap between the S$^{\text{v}}$ p-orbital and the Mo d_{xy} redox orbital.[29] Detailed spectroscopic and electronic structure studies on these and related complexes are currently underway and will address specific issues of Mo−S bond covalency as they relate to SO mediated catalysis.

Acknowledgment. This work was supported in part by funding from the NSF (Grant CHE-0216277 to M.L.K. and CHE-0202535 to C.J.C.) and the NIH. K.P. is supported by an NRSA fellowship (DK59724) from the NIH. Portions of this research were carried out at the Stanford Synchrotron Radiation Laboratory, a national user facility operated by Stanford University on behalf of the U.S. Department of Energy, Office of Basic Energy Sciences. The SSRL Structural Molecular Biology Program is supported by the Department of Energy, Office of Biological and Environmental Research, and by the National Institutes of Health, National Center for Research Resources, Biomedical Technology Program.

Supporting Information Available: Crystal coordinates and structure information for [(L3S)MoO(bdt)] and [(L3S)MoO(SPh)$_2$]. EXAFS spectra and fits for all of the complexes. This material is available free of charge via the Internet at http://pubs.acs.org.

IC034478Q